Impact of ΔB_0 field imperfections correction on BOLD sensitivity in 3D-SPARKLING fMRI data

Amor Zaineb[1], Le Ster Caroline[1], GR Chaithya[1,2], Daval-Frérot Guillaume[1,2,3], Thirion Bertrand[1,2], Boulant Nicolas[1], Mauconduit Franck[1], Mirkes Christian[4], Ciuciu Philippe[1,2], and Vignaud Alexandre[1]

[1]Université Paris-Saclay, CEA, NeuroSpin, CNRS, Gif-sur-Yvette, France
[2]Université Paris-Saclay, Inria, MIND, Palaiseau, France
[3]Siemens Healthineers SAS, Saint-Denis, France
[4]Skope Magnetic Resonance Technologies AG, Zurich, Switzerland

1 Synopsis

Static and dynamic ΔB_0 field imperfections are detrimental for fMRI applications as they degrade the temporal SNR (tSNR) and the sensitivity to the BOLD contrast. In this work we propose an experimental protocol for field imperfection monitoring and correction on 3D-SPARKLING fMRI data using the Skope Clip-on field camera in an alternative setting challenging its long TR constraint. We demonstrate the viability of our protocol and the reproducible gain in image quality, tSNR and retinotopic maps when correcting static and dynamic field imperfections on resting-state and task-based fMRI data for 3 healthy volunteers.

2 Summary of findings

The Skope Clip-on field camera can be used with a short TR if an external spoiling gradient is applied. Correcting field imperfections on 3D-SPARKLING fMRI data induces a highly significant improvement in image quality, tSNR and functional information.

3 Introduction

3D-SPARKLING is a novel non-Cartesian compressed sensing acquisition[1] recently assessed for high spatial resolution fMRI[2]. Similarly to its competitors, ΔB_0 imperfections affect 3D-SPARKLING data and cause BOLD sensitivity loss. Correcting field imperfections can be performed during image reconstruction given estimates of static inhomogeneities and their dynamic fluctuations[3].

A novel technology based on NMR probes [4, 5] that allows us to monitor field fluctuations concurrently to the imaging process has been gaining ground over the last years [6–8]. However, the minimal TR_{probe} required by this system is constrained by the T_1 relaxation time of the NMR-active product used and must be quite long to avoid residual magnetization between the consecutive shots. This is hardly achievable in a realistic 3D fMRI scenario where $TR_{probe} = TR_{shot}$.

In [8], the authors managed to use this system to acquire realistic 3D fMRI data with a short TR_{shot} and a long TR_{probe}: They assumed repeatable readouts between the shots, skipped monitoring some shots and interpolated the missing data. Such a strategy is impractical for 3D-SPARKLING applications given the random nature of the sampling pattern: In[9], we studied the benefit of correcting ΔB_0 imperfections on dynamic 3D-SPARKLING acquisitions without extending the study to realistic fMRI data because of the long TR_{probe} constraint.

In this work, we present an experimental protocol that allows us to use Skope's Clip-on Camera with $TR_{probe} = TR_{shot} = 50$ms and evaluate it for 1mm^3 3D-SPARKLING retinotopic mapping and rs-fMRI acquisitions.

4 Materials and methods

4.1 Experimental protocol and data acquisition

The study was conducted at 7T on three healthy volunteers (2M) who gave their informed consent. A 1Tx-32Rx head coil was used. Task-based and rs-fMRI data was collected using T_2^*w 3D-SPARKLING acquisitions[2]. A concomitantly retinotopic mapping protocol with a rotating wedge was run during task-based fMRI data acquisition. The code of the stimulation can be found in [1]. Additional ΔB_0 and sensitivity maps were acquired using a 3D GRE sequence. Zero'th and first-order field fluctuations were monitored over all shots using the Skope Clip-on Camera (Skope Magnetic Resonance Technologies AG, Zurich, Switzerland) and a $TR_{probe} = TR_{shots} = 50$ms. The residual magnetization resulting from the use of such a short TR_{probe} was eradicated using the highest spoiling gradient implementable within 3D-SPARKLING sequence(Fig. 1-(b)). The flip angle used to excite the probes yielded the highest signal.

4.2 Data reconstruction and post-processing

FMRI volumes were reconstructed using the calibrated multi-coil CS-based reconstruction method gueddari2 from the `pysap-mri` plugin[2] of the `pySAP` package sfarrens and the following extended received signal model

$$S(t) = e^{-2i\pi\Delta B_{0,dyn}\times t}\int_{\mathbf{r}\in\mathrm{FOV}} x(\mathbf{r})e^{-2i\pi\Delta B_{0,stat}(\mathbf{r})\times t}e^{-2i\pi(\mathbf{k}(t)+\delta\mathbf{k}(t))\cdot\mathbf{r}}\,d\mathbf{r}$$

[1] `https://github.com/hbp-brain-charting/public_protocols`
[2] `https://github.com/CEA_COSMIC/pysap-mri`

(a)

	TE (ms)	TR_{shot}(ms)	TR_{vol} (s)	Spatial resolution (mm)	FOV (mm)	Number of repetitions	Encoding direction
3D-SPARKLING	20	50	2.4	1mm iso	(192,192,128)	120 – 125	P-A
3D GRE	1.8, 3.06, 5.10	20	58	3mm iso	(192,192,132)	1	P-A
MP2RAGE	3.29	5000	347	1 mm iso	(192,192,128)	1	R-L

(b)

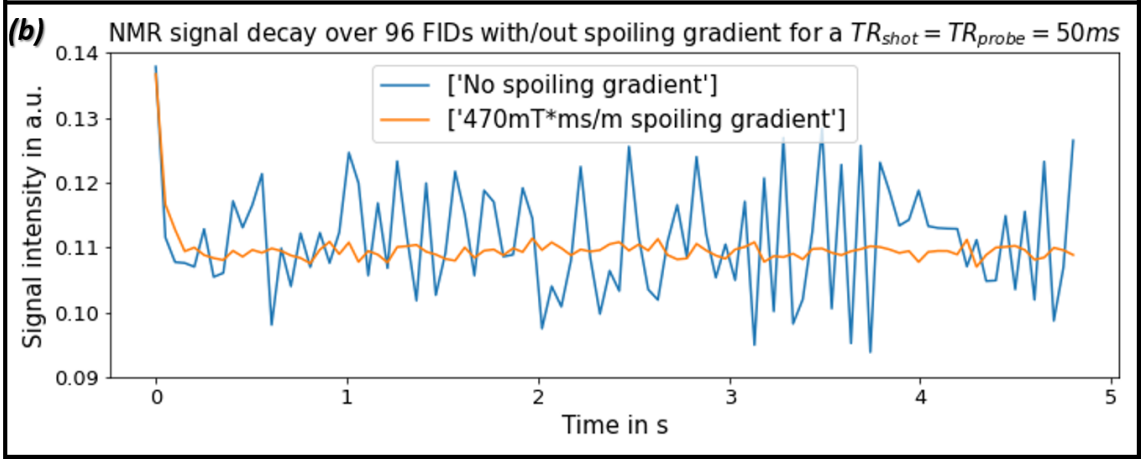

Figure 1: **(a)** Table summarizing the main sequences used for this experiment and their parameters: 3D-SPARKLING fMRI data was collected for a spatial resolution of 1mm^3 and a temporal resolution of 2.4s. A 3D gradient recalled echo (3D GRE) sequence with three echoes was used to acquire a ΔB_0 and external sensitivity maps. Raw data of the first echo from the GRE sequence was used to compute the sensitivity maps whereas the 3-echoe data was used to estimate the ΔB_0 map. A T_1w anatomical scan was acquired using an MP2RAGE sequence - **(b)** Example of the NMR signal decay from one probe of the Skope system over 96 FIDs with/out spoiling gradient for a $TR_{shots} = TR_{probe} = 50ms$.

with $x(\mathbf{r})$ the density source at the spatial position $\mathbf{r}$ and $\mathbf{k}(t)$ the k-space position at time t. $\Delta B_{0,stat}(\mathbf{r})$ denotes the static off-resonance effect at $\mathbf{r}$. $\Delta B_{0,dyn}$ and $\delta\mathbf{k}(t)$ denote the zero-th and first-order terms of the dynamic field fluctuations, respectively. We suppose $\Delta B_{0,dyn}$ to be constant during a shot.

Motion correction and co-registration of the fMRI and the T_1w anatomical data was performed using `SPM12`[3].

4.3 Statistical analysis

Resting-state data was used to compute the in vivo tSNR.

Retinotopic mapping data was analyzed using a subject-wise first-level GLM that included 2 paradigm-related regressors denoted α_1 and α_2, 6 motion regressors, a drift regressor, and the baseline. The global effect of interest and the BOLD phase maps were estimated as explained in Fig. 2.

[3] `https://www.fil.ion.ucl.ac.uk/spm/doc/biblio/`

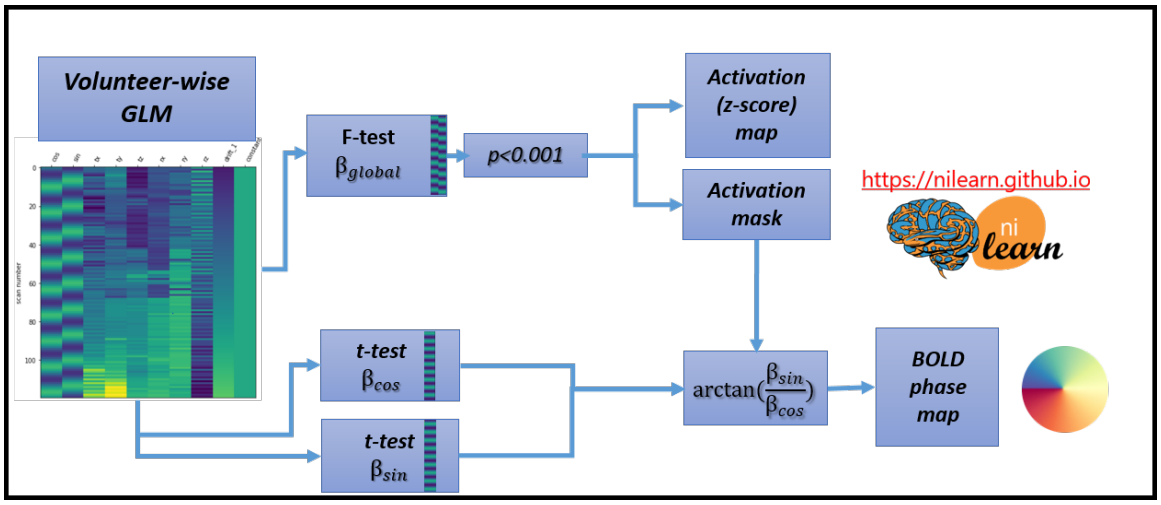

Figure 2: Statistical fMRI data analysis pipeline for retinotopic mapping: An F-test over the task regressors α_1 and α_2 was used to estimate the global effect of interest after thresholding the entire brain for $p < 0.001$ without correcting for multiple comparisons. The global effect of interest was thresholded at $p < 0.001$ to create activation masks. To estimate the BOLD phase, $\arctan(\frac{z_{\alpha_2}}{z_{\alpha_1}})$ was computed voxel-wise, z_{α_1} and z_{α_2} being the z-scores derived from a t-test over respectively α_1 and α_2. The phase maps were considered only on the regions of interest defined by the activation masks mentioned earlier.

5 Results

Fig. 1-(b) proves that steady state at the level of the probes FID signal is achievable using a $TR_{probe} = 50$ms and a 470mT*ms/m spoiling gradient.

Fig. 3 demonstrates the gain in image quality on corrected rs-fMRI data.

Fig. 4-(a) and (b) illustrate the tSNR improvement: We observed up to 34% gain in median tSNR when correcting the static contribution and up to the first-order dynamic terms. A significant improvement is observed in the visual cortex. Fig. 4-(c) shows the power spectrum of the $\Delta B_{0,dyn}$ term monitored during rs-fMRI for the 3 volunteers.

The tables in Fig. 5-(a) and (b) report a higher number of activated voxels as well as a higher significance (z-score max) on corrected task-based fMRI data.

Fig. 5-(c) shows improved and more significant activation maps when correcting field imperfections. Likewise, the BOLD phase maps in Fig. 5-(d) are more consistent with the color-gradient of the projection of the retina onto the visual cortex. This is mostly visible for z=-40: the transition from green to orange is more accurate when correcting field imperfections.

6 Discussion

Assuming that resting-state and task-based fMRI images are cleaned similarly when correcting ΔB_0 imperfections, the gain in tSNR observed in Fig. 4-(a) and (b) translates into a higher sensitivity to BOLD effect as supported by Fig. 5-(a) and (b).

In Fig. 5-(c), we can observe the emergence of some activations in white matter when correcting

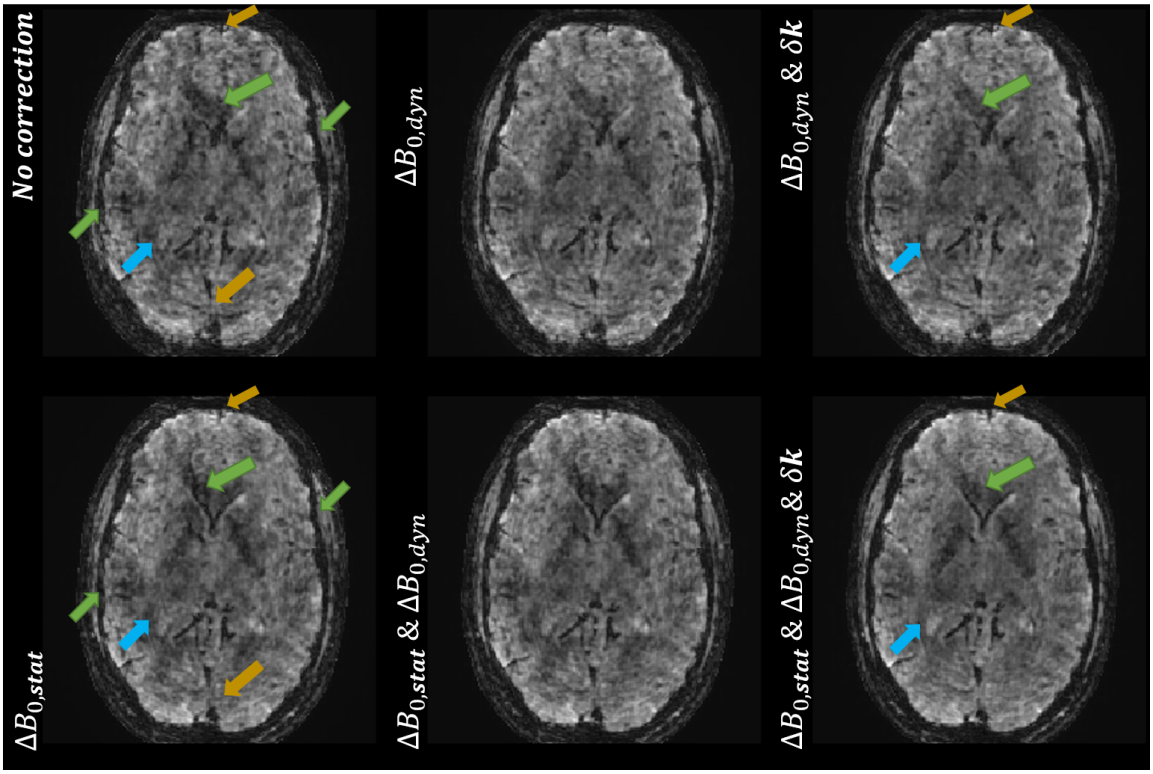

Figure 3: Comparison of the mean image of rs-fMRI time series for volunteer#1 with the correction of the different field terms. The overall contrast is enhanced when correcting the dynamic terms as shown by the blue arrow. Lost signal is better recovered when correcting both static and dynamic contributions as shown by the orange arrows. Anatomical details are better reconstructed as shown by the green arrows.

field imperfections(z=-40), yet, Fig. 5-(b) proves that the sensitivity to BOLD effect is significantly increased in gray matter and the better image quality of the corrected data observed in Fig. 3 suggests an improved effective spatial resolution.

The BOLD phase maps are also of a higher quality after field imperfections correction.

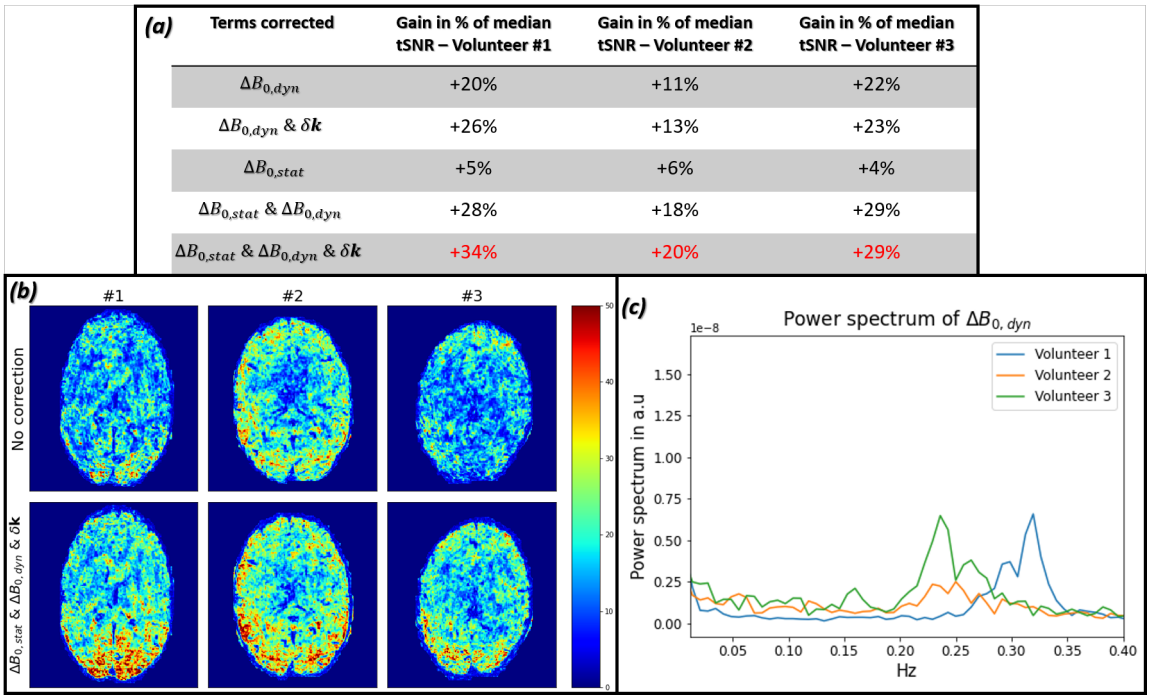

(a)

Terms corrected	Gain in % of median tSNR – Volunteer #1	Gain in % of median tSNR – Volunteer #2	Gain in % of median tSNR – Volunteer #3
$\Delta B_{0,dyn}$	+20%	+11%	+22%
$\Delta B_{0,dyn}$ & $\delta \boldsymbol{k}$	+26%	+13%	+23%
$\Delta B_{0,stat}$	+5%	+6%	+4%
$\Delta B_{0,stat}$ & $\Delta B_{0,dyn}$	+28%	+18%	+29%
$\Delta B_{0,stat}$ & $\Delta B_{0,dyn}$ & $\delta \boldsymbol{k}$	+34%	+20%	+29%

Figure 4: **(a)** Table summarizing the gain in % of median tSNR computed in comparison with the native tSNR (uncorrected data) for the three volunteers - **(b)** Temporal SNR maps extracted from rs-fMRI respectively uncorrected and corrected data displayed for the 3 volunteers - **(c)** Power spectrum of the $\Delta B_{0,dyn}$ term monitored during rsfMRI for the 3 volunteers. Only the range [0.12Hz, 0.4Hz] is displayed. We can observe the fluctuations due to breathing around 0.25-0.3Hz: Volunteer#2 has less intense breathing. Thus, the relative gain in % of median tSNR for this volunteer is lower than for the other two.

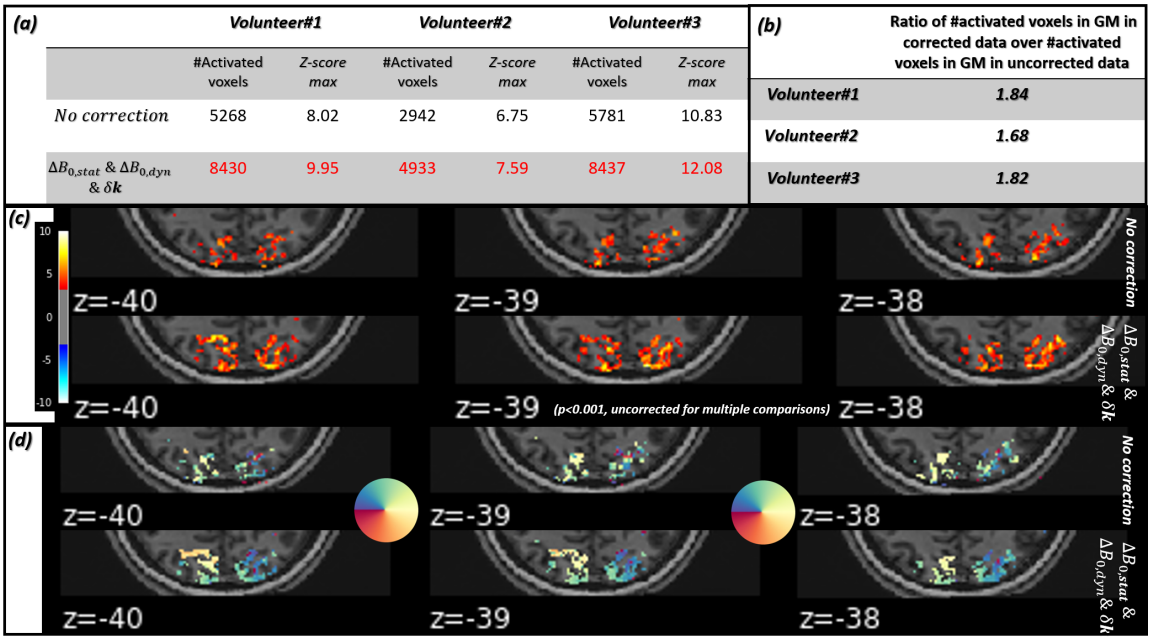

Figure 5: **(a)** Table summarizing the number of activated voxels and the maximum z-score values extracted from task-based fMRI data with/out correcting ΔB_0 imperfections. -**(b)** Table showing the increase in the number of activated voxels in gray matter extracted from task-based fMRI data after ΔB_0 imperfections correction. -**(c)** Activation maps extracted from the task-based uncorrected/corrected fMRI data collected from volunteer#1. -**(d)** BOLD phase maps extracted from the task-based uncorrected/corrected fMRI data collected from volunteer#1.

7 Conclusion

The Skope Clip-on Camera can be used with a short TR_{probe} if an external spoiling gradient is applied. Furthermore, the highly significant benefit we demonstrated on 3D-SPARKLING fMRI image quality, tSNR and BOLD sensitivity proves that the expected SNR loss in the probes FID signal due to the shorter TR does not degrade the accuracy of the estimated field fluctuations.

References

[1] C. G.R., P. Weiss, A. Massire, A. Vignaud, and P. Ciuciu, "Optimizing full 3D SPARKLING trajectories for high-resolution Magnetic Resonance imaging," *IEEE Transactions on Medical Imaging*, vol. 41, no. 8, pp. 2105–2117, Aug. 2022. DOI: 10.1109/TMI.2022.3157269.

[2] Z. Amor *et al.*, "Prospects of non-cartesian 3d-sparkling encoding for functional mri: A preliminary case: Study for retinotopic mapping," *Proceedings of the 30'th Scientific Meeting of the International Society for Magnetic Resonance in Medicine*, 2022.

[3] M. Doneva, "Mathematical models for magnetic resonance imaging reconstruction," *IEEE Signal Processing Magazine*, vol. 37, no. 1, pp. 24–32, 2020. DOI: 10.1109/MSP.2019.2936964.

[4] N. De Zanche, C. Barmet, J. A. Nordmeyer-Massner, and, "Nmr probes for measuring magnetic fields and field dynamics in mr systems," *Magnetic Resonance in Medecine*, vol. 60, no. 1, pp. 176–186, 2008. DOI: 10.1002/mrm.21624.

[5] C. Barmet, N. De Zanche, and K. P. Pruessmann, "Spatiotemporal magnetic field monitoring for mr. magnetic resonance in medecine," *Magnetic Resonance in Medecine*, vol. 60, no. 1, pp. 187–197, 2008. DOI: 10.1002/mrm.21603.

[6] S. J. Vannesjo *et al.*, "Retrospective correction of physiological field fluctuations in high-field brain mri using concurrent field monitoring," *Magnetic Resonance in Medecine*, vol. 73, no. 5, pp. 1833–1843, 2015. DOI: https://doi.org/10.1002/mrm.25303.

[7] S. Bollmann *et al.*, "Analysis and correction of field fluctuations in fmri data using field monitoring," *NeuroImage*, vol. 154, no. 1, pp. 92–105, 2017. DOI: 10.1016/j.neuroimage.2017.01.014.

[8] J. M. Schwarz, R. Stirnberg, P. Ehses, and T. Stocker, "Correction of physiological field fluctuations in high- and low-resolution 3d-epi acquisitions at 7 tesla," *Proceedings of the 27th Scientific Meeting of the International Society for Magnetic Resonance in Medicine*, 2019.

[9] Z. Amor *et al.*, "B field distortions monitoring and correction for 3d non-cartesian fmri acquisitions using a field camera: Application to 3d-sparkling at 7t," *Proceedings of the 30'th Scientific Meeting of the International Society for Magnetic Resonance in Medicine*, 2022.